

FORMATION OF CIRCUMBINARY PLANETS IN A DEAD ZONE

REBECCA G. MARTIN^{1,4}, PHILIP J. ARMITAGE^{1,2}, AND RICHARD D. ALEXANDER³

¹JILA, University of Colorado & NIST, UCB 440, Boulder, CO 80309, USA

²Department of Astrophysical and Planetary Sciences, University of Colorado, Boulder, CO 80309, USA

³Department of Physics & Astronomy, University of Leicester, Leicester, LE1 7RH, UK and

⁴NASA Sagan Fellow

Draft version July 31, 2018

ABSTRACT

Circumbinary planets have been observed at orbital radii where binary perturbations may have significant effects on the gas disk structure, on planetesimal velocity dispersion, and on the coupling between turbulence and planetesimals. Here, we note that the impact of all of these effects on planet formation is qualitatively altered if the circumbinary disk structure is layered, with a non-turbulent midplane layer (dead zone) and strongly turbulent surface layers. For close binaries, we find that the dead zone typically extends from a radius close to the inner disk edge up to a radius of around 10–20 au from the centre of mass of the binary. The peak in the surface density occurs within the dead zone, far from the inner disk edge, close to the snow line, and may act as a trap for aerodynamically coupled solids. We suggest that circumbinary planet formation may be *easier* near this preferential location than for disks around single stars. However, dead zones around wide binaries are less likely and hence planet formation may be more difficult there.

Subject headings: accretion, accretion disks — planets and satellites: formation — protoplanetary disks — stars: pre-main sequence — binaries: close

1. INTRODUCTION

The majority of Sun-like stars form in binary or multiple star systems (Duquennoy & Mayor 1991) and circumbinary disks result from their formation processes (e.g. Monin 2007; Kraus et al. 2012; Harris et al. 2012). The disks are similar to circumstellar disks but the central binary provides a torque on the inner edges of the disk that prevents the majority of the accretion flow on to the binary. Thus, circumbinary disks resemble decretion, rather than accretion, disks (Pringle 1981, 1991). These disks are the site for circumbinary planet formation.

There are currently at least thirteen circumbinary planets that have been observed. About half of these are around evolved stars (e.g. Thorsett, Arzoumanian & Taylor 1993; Parsons et al. 2010; Qian et al. 2010, 2012a,b). There are six planetary systems with a total of seven planets observed around main-sequence close binary stars (see Table 1). The planets in these systems lie at radii of only a few times the binary separation, where several physical effects are likely to make planet formation more difficult than at the equivalent radius in a circumstellar disk. First, the predicted collision velocities of planetesimals – if treated as test particles in a massless disk – are boosted by the secular eccentricity imparted from the binary (e.g. Moriwaki & Nakagawa 2004; Scholl, Marzari & Thébault 2007; Marzari, Thébault & Scholl 2008). The equilibrium eccentricity depends on the magnitude of gas drag, and is strongly suppressed by precession from even a moderately massive gas disk (Rafikov 2013). Nonetheless, estimates suggest that in situ formation of the observed circumbinary planets is unlikely; the observed planets must have formed farther out in the disk and migrated inwards (Paardekooper et al. 2012; Rafikov 2013). This scenario is supported by hydrodynamical simulations of the evolution of planetary cores (Pierens & Nelson 2007, 2008). Second, both the radial and non-axisymmetric structure (Marzari et al. 2012) of the

gas will be modified by the torque from the binary, altering both the aerodynamic migration of small solids and the Type I migration of planetary cores. Finally, it has been suggested that the interaction between the binary perturbation and stochastic planetesimal excitation from turbulence (Ida, Guillot & Morbidelli 2008) may lead to higher equilibrium eccentricities in circumbinary as compared to circumstellar disks (Meschiari 2012).

If a circumstellar or circumbinary disk is fully ionized, the magnetorotational instability (MRI) drives turbulence and angular momentum transport (Balbus & Hawley 1991). However, below a critical level of ionization, a dead zone may form at the midplane where the MRI does not operate (Gammie 1996; Armitage 2011). Surface layers of the disk may be ionized by cosmic rays or X-rays from the central stars (Glassgold, Najita & Igea 2004). The restricted flow through the disk causes a build up of material in the dead zone. Moreover, the quiescent dead zone layer allows solids to settle to the midplane and is thus a favourable formation site for planets.

In this work, we compute simplified models for poorly ionized circumbinary disks that contain dead zones. We show that all of the aforementioned physical processes that impact planet formation in circumbinary disks are strongly modified in dead zones, and argue that circumbinary planet formation may even be easier than circumstellar planet formation at particular disk radii.

2. CIRCUMBINARY DISK MODEL

In this Section we first describe the model consisting of a binary star with a coplanar¹ circular circumbinary disk orbiting the centre of mass of the stars. Then we describe results

¹ If the disk were to form strongly misaligned with the binary orbit, the timescale for realignment is short, about twenty orbital periods (Bate et al. 2000). Thus, we would only expect significant misalignment in the widest period binaries. We only consider models with an aligned binary and disk plane.

TABLE 1
SUMMARY OF OBSERVATIONS OF CIRCUMBINARY PLANETS AROUND MAIN-SEQUENCE STARS.

| Star System | M_1/M_\odot | M_2/M_\odot | a/au | e_b | Planet Name | M_p/M_J | a_p/au | e_p | Reference |
|-------------|---------------|---------------|---------------|--------|-------------|-------------|-----------------|---------|-----------|
| Kepler-16 | 0.654 | 0.1959 | 0.22 | 0.16 | b | 0.333 | 0.7048 | 0.0069 | 1,2 |
| Kepler-34 | 1.0479 | 1.0208 | 0.22 | 0.52 | b | 0.220 | 1.0896 | 0.18 | 3 |
| Kepler-35 | 0.8877 | 0.8094 | 0.18 | 0.14 | b | 0.127 | 0.6035 | 0.042 | 3 |
| Kepler-38 | 0.949 | 0.2492 | 0.1469 | 0.103 | b | 0.21 | 0.4644 | < 0.032 | 4 |
| Kepler-47 | 1.043 | 0.362 | 0.0836 | 0.0234 | b | ~ 0.03 | 0.2956 | < 0.035 | 5 |
| | | | | | c | ~ 0.06 | 0.989 | < 0.411 | 5 |
| Kepler-64 | 1.528 | 0.408 | 0.18 | | PH1 | 0.531 | 0.56 | 0.1 | 6, 7 |

NOTE. — Column 2 show the primary star mass, column 3 shows the secondary star mass, column 4 and 5 show the semi-major axis and eccentricity of the binary orbit respectively, column 7 shows the mass of the planet and columns 8 and 9 show the semi-major axis and eccentricity of the planet's orbit respectively.

REFERENCES. — (1) Doyle et al. (2011), (2) Bender et al. (2012), (3) Welsh et al. (2012), (4) Orosz et al. (2012a), (5) Orosz et al. (2012b), (6) Schwamb et al. (2012) and (7) Kostov et al. (2012).

from the simulations for various disk parameters.

2.1. Model Description

Previous work on circumbinary accretion disks has assumed the disk to be fully ionized and turbulent. We follow Alexander (2012) with the use of a one-dimensional circumbinary disk model but incorporate a layered disk model (Martin & Lubow 2011, 2013a; Lubow & Martin 2012, 2013). The disk is thermally ionized, and MRI active throughout, if the midplane temperature is greater than some critical value, $T_c > T_{\text{crit}}$. The value of the critical temperature is thought to be around 800 K (Umebayashi 1983), but we find that this temperature is not reached within the circumbinary disk. Below this temperature, the disk may become layered. The surface layers of the disk (with maximum surface density Σ_{crit}) are ionized by cosmic rays or X-rays from the central stars. If the total surface density is greater than the critical value, $\Sigma > \Sigma_{\text{crit}}$, then the active layers have surface density $\Sigma_m = \Sigma_{\text{crit}}$ and the midplane contains a dead zone with mass $\Sigma_d = \Sigma - \Sigma_{\text{crit}}$. If $\Sigma < \Sigma_{\text{crit}}$, then the whole disk is externally ionized and MRI active, $\Sigma_m = \Sigma$. This dead zone may become self gravitating if sufficient mass builds up such that the Toomre (1964) parameter, Q , is less than a critical value that we take to be 2. However, in this work, we find that there is not sufficient build up in a circumbinary disk for self-gravity.

The structure of the MRI active layer and the dead zone has not yet been well constrained. The surface density that is ionized by cosmic rays or X-rays, Σ_{crit} , has been calculated from the ionization balance of the external effects and internal effects such as Ohmic and ambipolar diffusion (e.g. Bai 2011; Simon et al. 2013). However, these calculations find accretion rates that are much lower than those observed in T Tauri stars, that require $\Sigma_{\text{crit}} > 10 \text{ g cm}^{-2}$ (e.g. Perez-Becker & Chiang 2011). With these uncertainties in mind, we allow Σ_{crit} to be a free parameter (e.g. Armitage, Livio & Pringle 2001; Zhu, Hartmann & Gammie 2009, 2010) and consider different values.

Material orbits the central binary of mass $M = M_1 + M_2$, at radius R , at Keplerian angular velocity, $\Omega = \sqrt{GM/R^3}$. The governing accretion disk equation, that includes a binary torque term, for the evolution of the total surface density $\Sigma = \Sigma_m + \Sigma_d$, and time t is

$$\frac{\partial \Sigma}{\partial t} = \frac{1}{R} \frac{\partial}{\partial R} \left\{ 3R^{1/2} \frac{\partial}{\partial R} \left[R^{1/2} (\nu_m \Sigma_m + \nu_d \Sigma_d) \right] - \frac{2\Lambda \Sigma R^{3/2}}{(GM)^{1/2}} \right\} \quad (1)$$

(Pringle 1981; Lin & Papaloizou 1986). The viscosity in the

MRI active surface layers is

$$\nu_m = \alpha_m \frac{c_m^2}{\Omega}, \quad (2)$$

where $\alpha_m = 0.01$ (e.g. Hartmann et al. 1998) is the Shakura & Sunyaev (1973) viscosity parameter, $c_m = \sqrt{\mathcal{R}T_m/\mu}$ is the sound speed, T_m is the temperature in the layer, \mathcal{R} is the gas constant and μ is the gas mean molecular weight. Similarly, the viscosity in the dead zone layer is

$$\nu_d = (\alpha_d + \alpha_g) \frac{c_s^2}{\Omega}, \quad (3)$$

where $c_s = \sqrt{\mathcal{R}T_c/\mu}$ is the sound speed at the midplane. The α_g term due to self-gravity is zero unless $Q < Q_{\text{crit}}$ (see Martin & Lubow 2011, for more details). MHD simulations suggest that there may be some residual viscosity in the dead zone and this is parameterised with α_d but it's value is still undetermined (e.g. Fleming & Stone 2003; Simon, Armitage & Beckwith 2011). We take $\alpha_d = 0$ in most of our models but consider one with a high value of $\alpha_d = 10^{-4}$ for comparison.

The tidal torque from the binary is

$$\Lambda(R, a) = \frac{q^2 GM}{2R} \left(\frac{a}{\Delta_p} \right)^4 \quad (4)$$

(Armitage et al. 2002), where $\Delta_p = \max(H, |R-a|)$, $H = c_s/\Omega$ is the disk scale height, a is the binary separation and $q = M_2/M_1$ is the mass ratio of the stars. Coupled with equation (1) we solve a simplified energy equation

$$\frac{\partial T_c}{\partial t} = \frac{2(Q_+ - Q_-)}{c_p \Sigma} \quad (5)$$

(Pringle, Verbunt & Wade 1986; Cannizzo 1993). The disk specific heat is $c_p = 2.7\mathcal{R}/\mu$. The local heating is

$$Q_+ = Q_\nu + Q_{\text{tid}} \quad (6)$$

where the viscous heating is

$$Q_\nu = \frac{9}{8} \Omega^2 (\nu_m \Sigma_m + \nu_d \Sigma_d) \quad (7)$$

and the tidal heating term is

$$Q_{\text{tid}} = (\Omega_b - \Omega) \Lambda \Sigma \quad (8)$$

(e.g. Lodato et al. 2009; Alexander et al. 2011), where the orbital frequency of the binary is $\Omega_b = \sqrt{GM/a^3}$. We also include a simple prescription for the effects of irradiation from

the central stars. We approximate the irradiation temperature of the disk with

$$T_{\text{irr}} = T_{\star} \left(\frac{2}{3\pi} \right)^{\frac{1}{4}} \left(\frac{R_{\star}}{R} \right)^{\frac{3}{4}} \quad (9)$$

(Chiang & Goldreich 1997), where we take $T_{\star} = 4000\text{ K}$ and $R_{\star} = 2R_{\odot}$. If the midplane temperature of the disk drops below the irradiation temperature then we assume that the disk is isothermal and $T_{\text{c}} = T_{\text{m}} = T_{\text{e}} = T_{\text{irr}}$ (see also Martin et al. 2012b). The cooling rate is

$$Q_{-} = \sigma T_{\text{e}}^4, \quad (10)$$

where T_{e} is the surface temperature of the disk and σ is the Stefan-Boltzmann constant. The temperature at the midplane, T_{c} , is related to the temperatures in the active layers, T_{m} , and at the surface, T_{e} , by considering the energy balance in the layered model above the midplane and is described with equations (6)-(12) in Martin et al. (2012b).

The binary torque clears the inner regions of the binary orbit (Artymowicz & Lubow 1994, 1996). It is strong enough to prevent all accretion flow into the binary region. Hence, the mass of the disk remains constant in time. However, some accretion may occur on to the binary through tidal streams. The maximum average of this is thought to be about ten per cent of the steady accretion flow (MacFadyen & Milosavljević 2008). Hence, we also include a model with accretion on to the binary stars. Material is removed from the inner regions of the disk at a fraction ϵ of the steady accretion rate $3\pi(\nu_{\text{m}}\Sigma_{\text{m}} + \nu_{\text{g}}\Sigma)$.

The initial surface density is chosen to be

$$\Sigma = \Sigma_0 \left(\frac{R_0}{R} \right) \exp\left(-\frac{R}{R_0}\right), \quad R > 10a, \quad (11)$$

where we take $R_0 = 15a$ and scale the constant Σ_0 such that the total mass of the disk, M_{disk} , is equal to some constant in the range $0.01 - 0.1 M_{\odot}$ (see also Alexander 2012). This initial condition has little effect on the structure of the disk at later times. The total mass of the disk, not the initial distribution of mass, is the important feature.

We take a grid of 200 points distributed evenly in $\log R$ from $R_{\text{in}} = 2a$ up to $R_{\text{out}} = 1000\text{ AU}$. At the inner edge we have a zero surface density inner boundary condition, but because the binary torque is strong, there is no material here. At the outer edge we take a zero radial velocity boundary condition to prevent mass loss, but we have chosen a radius large enough that no significant amount of material spreads this far in a reasonable timescale. In the following section we describe the results of our simulations.

2.2. Model Results

Fig. 1 shows the disk structure for two circumbinary disk models with central binary star masses of $M_1 = 1 M_{\odot}$ and $M_2 = 1 M_{\odot}$ with a separation $a = 0.2\text{ au}$, accretion efficiency $\epsilon = 0$ and total disk mass $M_{\text{disk}} = 0.05 M_{\odot}$. Model R1 is fully turbulent and model R2 has a dead zone defined by $\Sigma_{\text{crit}} = 20\text{ g cm}^{-2}$. In both cases, the inner parts of binary region are cleared out to a radius of greater than 1 au . In model R2, the dead zone structure is set up in less than 10^5 yr and then is fairly constant in time. The disk is fully MRI turbulent in the inner and outer parts where the surface density is less than the critical that is ionized by external sources, $\Sigma < \Sigma_{\text{crit}}$. The dead zone extends from 1.91 au to 18.5 au at a time of 3 Myr ,

for example, and is not self gravitating at any time. The mass of the dead zone decreases in time as the disk spreads out in radius. The peak in the surface density distribution is much farther from the binary star in the disk with a dead zone, than in the fully turbulent case where the peak is close to the inner edge of the disk. The radius of the peak surface density moves inwards in time. We discuss this feature further in Section 2.3.

Similarly, the peak in the temperature distribution of the fully turbulent disk is closer to the binary star than the disk with a dead zone. The snow line radius, R_{snow} , is the radius beyond which ice condenses from the disk, that occurs at a temperature of around $T_{\text{snow}} = 170\text{ K}$ (e.g. Lecar et al. 2006; Martin & Livio 2012, 2013). Thus, the snow line temperature occurs at a radius farther from the binary in the disk with a dead zone. Because the solid mass density is much larger beyond the snow line, planetesimal formation is much easier there and thus giant planets may form more easily. Hence we expect both gas giants and rocky terrestrial planets to form in circumbinary disks, as they do in circumstellar disks. In the dead zone model, terrestrial planet formation is easier compared with the turbulent model as there is a larger radius out to which they can form.

In Table 2 we show models with various disk parameters and find that the dead zone is extensive for a range of disk masses and critical surface densities. The smaller the critical surface density, Σ_{crit} , the larger the dead zone and the larger the radius of the peak surface density (comparing models R2 and R4, for example). If the disk mass is small (less than $0.05 M_{\odot}$), the critical surface density must be small, ($\Sigma_{\text{crit}} < 20\text{ g cm}^{-2}$) for a dead zone to exist for the whole disk lifetime, up to 10 Myr (see models R6 and R7). On the other hand, if the disk is massive, the dead zone is more extensive and the peak surface density is at a larger radius (see model R8). The accretion flow from the disk on to the binary (model R5 with $\epsilon > 0$) has little effect on the structure of the disk and the dead zone. In this case, the average accretion rate on to the binary stars is $6.5 \times 10^{-10} M_{\odot} \text{ yr}^{-1}$.

2.3. Peak Surface Density

For a disk without a dead zone, the maximum surface density occurs close to the inner edge of the disk, as shown in the top plots of Fig. 1. However, in a disk that contains a dead zone, the peak surface density may lie far from the inner edge (see Table 2).

The inner parts of the circumbinary disk show little radial movement over the lifetime of the disk (as shown in Fig. 1). In such a disk the inward or outward movement of dust particles is determined by the sign of the radial pressure gradient (e.g. Takeuchi & Lin 2002, 2005). The pressure gradient, $\partial P / \partial R$, where $P = c_s^2 \Sigma / \sqrt{2\pi} H$, is positive inside of the radius of the peak surface density, R_{peak} , and negative outside. This suggests that particles of all sizes drift towards and collect around this radius. The radius of the peak surface density occurs far from the inner edge of the disk for models with a dead zone. It moves outwards with decreasing active layer surface density.

Paardekooper et al. (2012) found that planetesimal accretion can occur in $R > 20a = 4.4\text{ au}$ for Kepler-16, $R > 12a = 2.64\text{ au}$ for Kepler-34 and $R > 15a = 2.7\text{ au}$ for Kepler-35. The results of Rafikov (2013) suggest that these numbers may overstate the difficulty of forming planetesimals, at least while the gas disk remains relatively massive. Models R9 and R10 represent the specific example of Kepler-16. Models R1–R8 represent circumbinary disk models for Kepler-34 and Kepler-

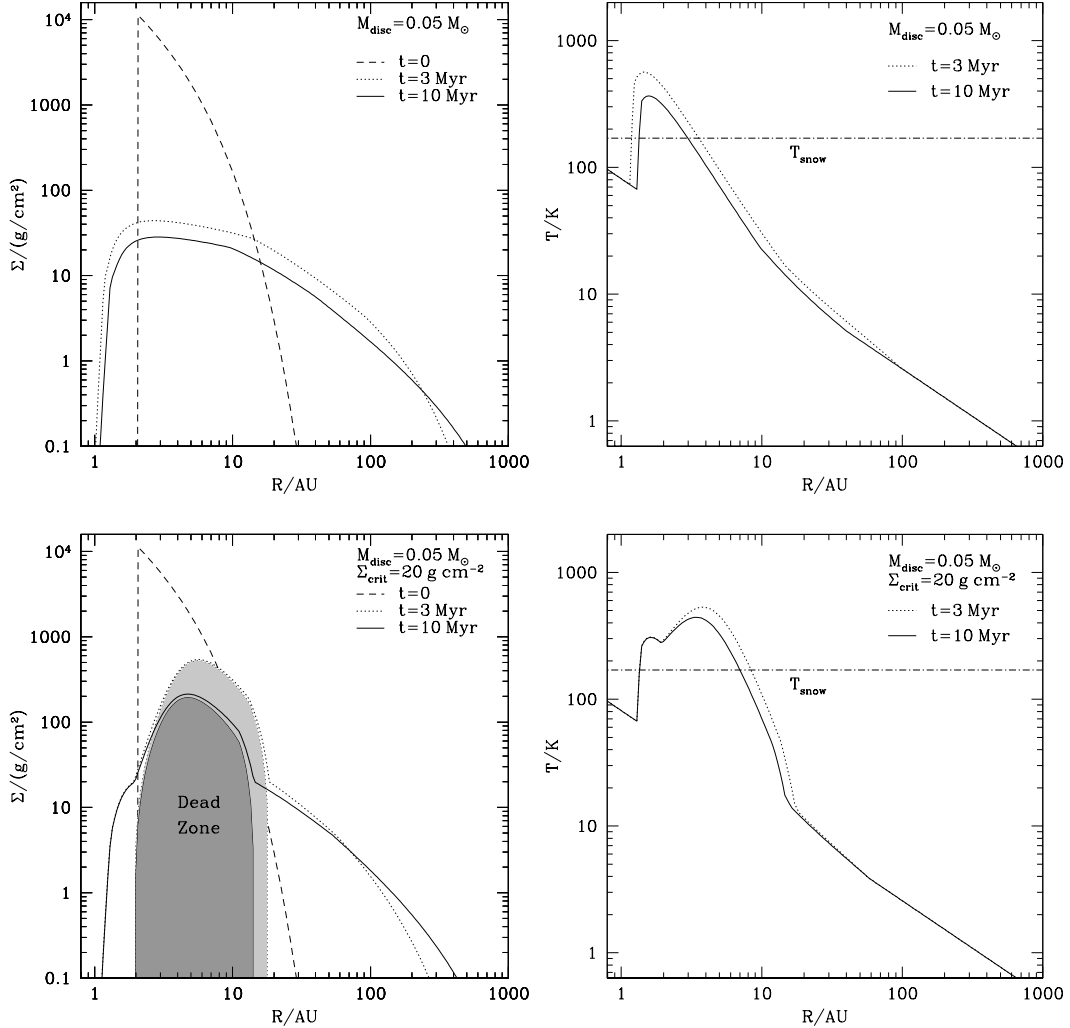


FIG. 1.— The disk surface density (left) and central temperature (right) at a time of $t = 3$ Myr (dotted lines) and 10 Myr (solid lines) for a fully turbulent circumbinary disk (model R1, upper plots) and a disk with a dead zone defined by $\Sigma_{\text{crit}} = 20 \text{ g cm}^{-2}$ (model R2, lower plots). The dashed lines in the surface density plots show the initial surface density. The shaded regions shows the surface density of the dead zone at $t = 3$ Myr (pale shaded region) and $t = 10$ Myr (dark shaded region). The dot-dashed lines in the temperature plots show the snow line temperature.

35. For reasonable dead zone models, we find that the peak surface density is farther out than the region where planetesimal accretion is inhibited. Thus, the dead zone is a likely formation site for the circumbinary planets. The binary perturbations do not affect planetesimal growth in a circumbinary disk with a dead zone.

2.4. Viscosity in the Dead Zone

A non-zero viscosity in the the dead zone is uncertain and thus we have assumed that the dead zone has zero turbulence, $\alpha_d = 0$, in most of our models. However, shearing box simulations suggest that the MHD turbulence generated in the disk surface layers may produce some hydrodynamic turbulence in the dead zone layer that may produce a small but non-zero viscosity (e.g. Fleming & Stone 2003; Simon, Armitage & Beckwith 2011; Gressel, Nelson & Turner 2012).

With this uncertainty in mind we also performed one simulation with a viscosity in the dead zone, model R3. We choose the parameters of model R2 but include a viscous term in the dead zone with $\alpha_d = 10^{-4}$. We note that this is likely to be an

upper limit to the viscosity in the dead zone. In a circumstellar accretion disk, the amount of mass flow through the dead zone should be less than that through the active layer because the turbulence in the dead zone is generated by the turbulence in the active layers (see also Bae et al. 2013). Even in this extreme case we find that the disk structure is not significantly altered. The extent of the dead zone is actually larger, but the mass in the dead zone is slightly smaller. The peak in the surface density occurs at a radius slightly closer to the binary stars, but still farther out than the region that is hostile to planetesimal formation for Kepler-34 and Kepler-35. If the magnitude of the viscosity in the dead zone is reduced by a factor of around ten or more then the effect on our results is minimal. Thus, we conclude that a small but non-zero viscosity in the dead zone will not significantly affect the results presented here.

2.5. Wide Separation Binaries

The table also includes some circumbinary disk models for larger separation binaries (models R11–R13). Here, the surface density of the disk (and thus the mass) must be much

TABLE 2
SUMMARY OF CIRCUMBINARY DISKS MODELS.

| Model | M_1 (M_\odot) | M_2 (M_\odot) | a (au) | Σ_{crit} (g cm^{-2}) | α_d | ϵ | M_{disk} (M_\odot) | M_{DZ} (M_\odot) | R_{d1} (au) | R_{d2} (au) | R_{peak} (au) | R_{peak} (au) | M_{disk} (M_\odot) | M_{DZ} (M_\odot) | R_{snow} (au) |
|----------|------------------------|------------------------|-------------|--|------------|------------|------------------------------------|----------------------------------|------------------|------------------|---------------------------|---------------------------|------------------------------------|----------------------------------|---------------------------|
| Time/Myr | all | | | | | | 0 | 3 | | | | 10 | | | |
| R1 | 1.0 | 1.0 | 0.2 | > 44 | 0.0 | 0.0 | 0.05 | - | - | - | 2.72 | 2.94 | 0.05 | - | 2.94 |
| R2 | 1.0 | 1.0 | 0.2 | 20 | 0.0 | 0.0 | 0.05 | 0.0231 | 1.91 | 18.5 | 5.72 | 4.70 | 0.05 | 0.00575 | 5.95 |
| R3 | 1.0 | 1.0 | 0.2 | 20 | 10^{-4} | 0.0 | 0.05 | 0.0179 | 1.77 | 20.8 | 4.70 | 4.35 | 0.05 | 0.00349 | 5.29 |
| R4 | 1.0 | 1.0 | 0.2 | 10 | 0.0 | 0.0 | 0.05 | 0.0369 | 1.91 | 21.6 | 7.82 | 7.52 | 0.05 | 0.0249 | 9.15 |
| R5 | 1.0 | 1.0 | 0.2 | 20 | 0.0 | 0.1 | 0.05 | 0.0202 | 1.91 | 18.5 | 5.50 | 4.35 | 0.0435 | 0.00243 | 5.09 |
| R6 | 1.0 | 1.0 | 0.2 | 20 | 0.0 | 0.0 | 0.02 | 0.00208 | 1.99 | 11.6 | 4.35 | 3.18 | 0.02 | - | - |
| R7 | 1.0 | 1.0 | 0.2 | 10 | 0.0 | 0.0 | 0.02 | 0.00994 | 1.91 | 17.1 | 6.69 | 5.72 | 0.02 | 0.00328 | 5.72 |
| R8 | 1.0 | 1.0 | 0.2 | 20 | 0.0 | 0.0 | 0.1 | 0.0669 | 1.70 | 22.5 | 6.43 | 5.94 | 0.1 | 0.0381 | 9.15 |
| R9 | 0.7 | 0.2 | 0.2 | 20 | 0.0 | 0.0 | 0.05 | 0.0362 | 1.06 | 12.0 | 4.02 | 3.72 | 0.05 | 0.0249 | 5.72 |
| R10 | 0.7 | 0.2 | 0.2 | 10 | 0.0 | 0.0 | 0.05 | 0.0435 | 1.20 | 12.0 | 5.29 | 5.09 | 0.05 | 0.0375 | 6.43 |
| R11 | 1.0 | 1.0 | 1.0 | > 13.3 | 0.0 | 0.0 | 0.05 | - | - | - | 12.5 | 12.9 | 0.05 | - | - |
| R12 | 1.0 | 1.0 | 2.0 | > 5.8 | 0.0 | 0.0 | 0.05 | - | - | - | 24.7 | 25.4 | 0.05 | - | - |
| R13 | 1.0 | 1.0 | 5.0 | > 2.0 | 0.0 | 0.0 | 0.05 | - | - | - | 60.3 | 63.1 | 0.05 | - | - |

NOTE. — Column 2 shows the mass of the primary star, column 3 shows the mass of the secondary star and column 4 shows the semi-major axis of the binary orbit. Column 5 shows the critical surface density that is ionized by cosmic rays or X-rays from the central binary and column 6 shows the viscosity parameter in the dead zone. Column 7 shows the parameter ϵ that describes the efficiency of accretion on to the binary and column 8 shows the initial mass of the disk. Columns 9-12 describe the disk structure at a time $t = 3$ Myr. Column 9 shows the mass of the dead zone, columns 10 and 11 show the inner and outer radius of the dead zone, respectively and column 12 shows the radius of the peak surface density. Columns 13-16 describe the disk structure at $t = 10$ Myr. Column 13 shows the radius of the peak surface density, column 14 shows the disk mass, column 15 shows the dead zone mass and column 16 shows the radius of the snow line. In rows where there is no snow line radius shown, the snow line is inside the inner edge of the disk.

larger for a dead zone to be present. For an equal mass binary with a separation of 1 au, the peak surface density is only 13.3 g cm^{-2} (at a time of 3 Myr, see model R11) and this decreases with binary separation (see for example models R12 and R13). If a dead zone is required for planet formation, this suggests that circumbinary planet formation is far more likely in close binaries.

3. DISCUSSION

When a massive planet forms within a disk, it can open a gap in the disk. The gap opening mass, according to the viscous criterion (Lin & Papaloizou 1986), will be significantly reduced in a dead zone, but the thermal criterion will be only modestly affected. Even in a normal circumstellar accretion disk, this mass is well below a Jupiter mass (Zhu, Stone & Rafikov 2013) and for the most massive planets to form, there must be accretion on to the planet across the gap (Lubow & D’Angelo 2006). The planet captures most of the material that flows across the gap and the dead zone does not drastically affect planetary accretion in a circumstellar disk (Uribe, Klahr & Henning 2013). However, in a circumbinary disk, there is very little mass flow and thus it is not clear how much accretion would occur on to a planet in this case. If the accretion is reduced significantly compared with a circumstellar accretion disk, then we would expect only lower mass gas giants to form within circumbinary disks. However, this should be investigated in future work. Similarly, the presence of the dead zone with a highly reduced viscosity will mean that migration timescales are significantly different than in the turbulent disk.

If planets form within the dead zone, thus removing the mass from the disk, the remaining disk may have a sufficiently low surface density that the whole disk becomes fully turbulent. Thus, the remaining turbulent disk may accrete on to the planetary cores allowing the formation of giant planets in the late stages of disk evolution.

There are a number of improvements that should be made to this disk model in future, such as modelling the non-

axisymmetric tidal streams, non-axisymmetric stellar irradiation and increasing the eccentricity or inclination of the binary orbit. The models presented here cannot model such effects, but are a first step towards understanding the formation of dead zones in circumbinary disks. If a dead zone is present in a circumbinary disk, then it remains for the lifetime of the disk. This is because the binary torque is preventing the majority of accretion and the mass of the disk is fairly constant. The dead zone evolves on a long timescale. However, in the circumstellar disk, once the infall accretion rate drops, the dead zone may be accreted and the cosmic rays or X-rays can penetrate the whole of the less massive disk. This suggests that planet formation in close binary stars is even more likely in circumbinary disks despite the concerns about planetesimal accretion in the innermost regions.

A more realistic way to measure the extent of the dead zone may be with a critical magnetic Reynolds number (e.g. Fromang, Terquem & Balbus 2002; Matsumura & Pudritz 2003). The active layer surface density then varies with radius (e.g. Martin et al. 2012a). However, models with this prescription cannot account for the accretion rates observed in T Tauri stars and this issue is yet to be resolved.

We note also that our model does not account for mass-loss due to photoevaporation. Photoevaporative winds are thought to drive final disk clearing in disks around single stars (e.g. Alexander, Clarke & Pringle 2006; Gorti, Dullemond & Hollenbach 2009; Owen et al. 2010). However, Alexander (2012) showed that, because accretion is suppressed by the tidal torque from the binary, photoevaporation plays a much larger role in the evolution of circumbinary disks. Photoevaporation steadily erodes material from near the disk inner edge, and can modify the disk structure significantly if the mass-loss rate is high enough. Moreover, for the close binary separations considered here much of the photoevaporative mass-loss comes from \sim AU radii, similar to the locations of our predicted dead zones. Crudely, we expect photoevaporative mass-loss to shorten the lifetimes of the dead zone, and perhaps also to modify the radial surface den-

sity profile at radii $\lesssim 10\text{AU}$. However, the interplay between photoevaporation and layered accretion can be subtle even in single-star disks (Morishima 2012), and detailed investigation of this issue is beyond the scope of this paper.

The increased surface density in the dead zone (compared to a fully turbulent model) may lead to damping of the perturbations to the planetesimals from the binary torque. For example, for a fixed disk aspect ratio, H/r , the drag force increases linearly with the surface density (e.g. Marzari & Scholl 2000). Because the drag force is also inversely proportional to the particle size, comparing the effect of particle sizes is equivalent to comparing varying surface density. The larger the particle size the larger the damping and thus we expect the increased surface density in the dead zone to increase the damping. The effect of the large surface density in the dead zone on the planetesimal perturbations should be investigated further in future work.

4. CONCLUSIONS

With circumbinary disk models we find a dead zone typically extends from a radius close to the inner disk edge up to a radius of around 10–20 au for a close binary. The dead zone provides a quiescent region where solids can settle to the mid-plane, ideal for planet formation. A peak in the surface density occurs in the dead zone, far from the inner disk edge, and dust particles of all sizes drift towards this radius. Thus, the binary torque, that makes the inner regions of the disk hostile to planetesimal accretion, may not affect the growth of plan-

etesimals in a disk with a dead zone. The currently observed circumbinary planets likely formed in such a region before their inward migration to their current location. The snow line typically occurs close to but slightly outside of the peak in the surface density. Thus, we expect both massive gas giants and terrestrial planets to form in such disks. Because the binary provides a torque on the disk preventing accretion, the dead zone is not accreted on to the binary and lasts the lifetime of the disk. Thus, planet formation may be even more likely in circumbinary disks around close binaries than in circumstellar disks. Dead zones around wide binaries are less likely and thus we suggest planet formation may be more difficult there.

ACKNOWLEDGEMENTS

We thank an anonymous referee for useful comments. RGM's support was provided in part under contract with the California Institute of Technology (Caltech) funded by NASA through the Sagan Fellowship Program. PJA acknowledges support from NASA under grant HST-AR-12814 awarded by the Space Telescope Science Institute, which is operated by the Association of Universities for Research in Astronomy, Inc., for NASA, under contact NAS 5-26555, and from NASA's Origins of Solar Systems program under grant NNX13AI58G. RDA acknowledges support from the Science & Technology Facilities Council (STFC) through an Advanced Fellowship (ST/G00711X/1) and Consolidated Grant ST/K001000/1.

REFERENCES

- Alexander R. D., Clarke C. J., Pringle J. E., 2006, *MNRAS*, 369, 229
- Alexander R. D., Wynn G. A., King A. R., Pringle J. E., 2011, *MNRAS*, 418, 2576
- Alexander R. D., 2012, *ApJ*, 757, 29
- Armitage P. J., 2011, *ARA&A*, 49, 195
- Armitage P. J., Livio M., Pringle J. E., 2001, *MNRAS*, 324, 705
- Armitage P. J., Livio M., Lubow S. H., Pringle J. E., 2002, *MNRAS*, 334, 248
- Artymowicz P., Lubow S. H., 1994, *ApJ*, 421, 651
- Artymowicz P., Lubow S. H., 1996, *ApJ*, 467, L77
- Bae J., Hartmann L., Zhu Z., Gammie C., 2013, *ApJ*, 764, 141
- Bai X.-N., 2011, *ApJ*, 739, 50
- Balbus S. A., Hawley J. F., 1991, *ApJ*, 376, 214
- Bate M. R., Bonnell I. A., Clarke C. J., Lubow S. H., Ogilvie G. I., Pringle J. E., Tout C. A., 2000, *MNRAS*, 317, 773
- Bender C. F., Mahadevan S., Deshpande R., 2012, *ApJ*, 751, L31
- Cannizzo, J. K. 1993, *ApJ*, 419, 318
- Chiang E. I., Goldreich P., 1997, *ApJ*, 490, 368
- Doyle L. R., Carter J. A., Fabrycky D. C., et al., 2011, *Sci*, 333, 1602
- Duquennoy A., Mayor M., 1991, *A&A*, 248, 485
- Fleming T., Stone J. M., 2003, *ApJ*, 585, 908
- Fromang S., Terquem C., Balbus S. A., 2002, *MNRAS*, 329, 18
- Gammie C. F., 1996, *ApJ*, 457, 355
- Glassgold A. E., Najita J., Igea J., 2004, *ApJ*, 615, 972
- Gorti U., Dullemond C. P., Hollenbach D., 2009, *ApJ*, 705, 1237
- Gressel, O., Nelson R. P., Turner N. J., 2012, *MNRAS*, 422, 1140
- Harris R. J., Andrews S. M., Wilner D. J., Kraus A. L., 2012, *ApJ*, 751, 115
- Hartmann L., Calvet N., Gullbring E., D'Alessio P., 1998, *ApJ*, 495, 385
- Ida S., Guillot T., Morbidelli A., 2008, *ApJ*, 686, 1292
- Kostov V. B., McCullough P. R., Hinse T. C., Tsvetanov Z. I., Hébrard G., Diaz R. F., Deleuil M., Valenti J. A., 2013, *ApJ*, 770, 52
- Kraus A. L., Ireland M. J., Hillenbrand L. A., Martinache F., 2012, *ApJ*, 745, 19
- Lecar M., Podolak M., Sasselov D., Chiang E., 2006, *ApJ*, 640, 1115
- Lodato G., Nayakshin S., King A. R., Pringle J. E., 2009, *MNRAS*, 398, 1392
- Lin D. N. C., Papaloizou J., 1986, *ApJ*, 309, 846
- Lubow S. H., D'Angelo G., 2006, *ApJ*, 641, 526
- Lubow S. H., Martin R. G., 2012, *ApJ*, 749, L37
- Lubow S. H., Martin R. G., 2013, *MNRAS*, 428, 2668
- MacFadyen A. I., Milosavljević M., 2008, *ApJ*, 672, 83
- Martin R. G., Lubow S. H., 2011, *ApJ*, 740, L6
- Martin R. G., Lubow S. H., Livio M., Pringle J. E., 2012a, *MNRAS*, 420, 3139
- Martin R. G., Lubow S. H., Livio M., Pringle J. E., 2012b, *MNRAS*, 423, 2718
- Martin R. G., Livio M., 2012, *MNRAS*, 425, L6
- Martin R. G., Lubow S. H., 2013, *MNRAS*, 432, 1616
- Martin R. G., Livio M., 2013, *MNRAS*, 428, L11
- Marzari F., Scholl H., 2000, *ApJ*, 543, 328
- Marzari F., Thébault P., Scholl H., 2008, *ApJ*, 681, 1599
- Marzari F., Baruteau C., Scholl H., Thébault P., 2012, *A&A*, 539, 98
- Matsumura S., Pudritz R. E., 2003, *ApJ*, 598, 645
- Meschiari S., 2012, *ApJ*, 761, L7
- Monin J. L., Clarke C. J., Prato L., McCabe C., 2007, in *Protostars and Planets V*, ed. B. Reipurth, D. Jewitt, K. Keil, Tucson AZ, Univ. Arizona Press, 395
- Morishima R., 2012, *MNRAS*, 420, 2851
- Moriwaki K., Nakagawa Y., 2004, *ApJ*, 609, 1065
- Orosz J. A., Welsh W. F., Carter J. A., et al., 2012a, *ApJ*, 758, 87
- Orosz J. A., Welsh W. F., Carter J. A., et al., 2012b, *Sci*, 337, 1511
- Owen J. E., Ercolano B., Clarke C. J., Alexander R. D., 2010, *MNRAS*, 401, 1415
- Paardekooper S., Leinhardt A. M., Thébault P., Baruteau C., 2012, *ApJ*, 754, L16

- Parsons S. G., Marsh T. R., Copperwheat C. M., Dhillon V. S., Littlefair S. P., Gänsicke B. T., Hickman R., 2010, *MNRAS*, 402, 2591
- Perez-Becker D., Chiang E., 2011, *ApJ*, 727, 2
- Pierens A., Nelson R. P., 2007, *A&A*, 472, 993
- Pierens A., Nelson R. P., 2008, *A&A*, 483, 633
- Pringle J. E., 1981, *ARA&A*, 19, 137
- Pringle J. E., 1991, *MNRAS*, 248, 754
- Pringle J. E., Verbunt F., Wade, R. A. 1986, *MNRAS*, 221, 169
- Qian S. B., Liao W. P., Zhu L. Y., Dai Z. B., 2010, *ApJ*, 708, L66
- Qian S. B., Zhu L. Y., Dai Z. B., Fernández-Lajús E., Xiang F. Y., He J. J., 2012a, *ApJ*, 745, L23
- Qian S. B., Liu L., Zhu L. Y., Dai Z. B., Fernández Lajús E., Baume, G. L., 2012, *MNRAS*, 422, L24
- Rafikov R. R., 2013, *ApJL*, submitted, arXiv:1212.2217
- Scholl H., Marzari F., Thébault P., 2007, *MNRAS*, 380, 1119
- Schwamb M. E., Orosz J. A., Carter J. A., et al., 2013, *ApJ*, 768, 127
- Shakura N. I., Sunyaev R. A., 1973, *A&A*, 24, 337
- Simon J. B., Armitage P. J., Beckwith K., 2011, *ApJ*, 743, 17
- Simon J. B., Bai X., Stone J. M., Armitage P. J., Beckwith K., 2013, *ApJ*, 764, 66
- Takeuchi T., Lin D. N. C., 2002, *ApJ*, 581, 1344
- Takeuchi T., Lin D. N. C., 2005, *ApJ*, 623, 482
- Thorsett S. E., Arzoumanian Z., Taylor J. H., 1993, *ApJ*, 412, L33
- Toomre A., 1964, *ApJ*, 139, 1217
- Umebayashi T., 1983, *Progress Theor. Phys.*, 69, 480
- Uribe A. L., Klahr H., Henning T., 2013, *ApJ*, 769, 97
- Welsh W. F., Orosz J. A., Carter J. A., et al., 2012, *Nature*, 481, 475
- Zhu Z., Hartmann L., Gammie C., 2009, *ApJ*, 694, 1045
- Zhu Z., Hartmann L., Gammie C., 2010, *ApJ*, 713, 1143
- Zhu Z., Stone J. M., Rafikov R., 2013, *ApJ*, 768, 143